Journal of Materials Chemistry B

ROYAL SOCIETY OF CHEMISTRY

PAPER

View Article Online
View Journal | View Issue



Cite this: J. Mater. Chem. B, 2021, 9, 5069

# Cascade catalytic nanoplatform constructed by laterally-functionalized pillar[5]arenes for antibacterial chemodynamic therapy†

Fei Li,‡[a] Mingsong Zang,‡[a] Jinxing Hou,[a] Quan Luo,[a] Shuangjiang Yu,[b] Hongcheng Sun,[b] Jiayun Xu*[ab] and Junqiu Liu*[ab]

Received 17th April 2021,
Accepted 30th May 2021

DOI: 10.1039/d1tb00868d

rsc.li/materials-b

Chemodynamic therapy (CDT) is an emerging approach to overcome bacterial infections that can efficiently convert hydrogen peroxide ($H_2O_2$) to generate highly toxic hydroxyl radicals (•OH). How to develop safe and effective CDT-based strategies is in high demand but challenging. Herein, a cascade catalytic nanoplatform (GOx–NCs/$Fe_3O_4$) was designed by absorbing glucose oxidase (GOx) onto the surface of covalent-assembled polymer capsules (NCs) encapsulating $Fe_3O_4$ nanoparticles. With the presence of glucose, GOx could effectively catalyze it to produce $H_2O_2$ and result in a decrease in pH value, both of which would assist the subsequent Fenton reaction. Encapsulated $Fe_3O_4$ nanoparticles would subsequently trigger $H_2O_2$ to produce •OH, which could make antibacterial CDT come true. More importantly, the polymer capsules exhibited little to no cytotoxicity towards mammalian cells, which might provide more opportunities and potential to apply in other fields.



## Introduction

Bacterial infections have more and more become a severe challenge and threat to human life.[1–8] To deal with the current situation of drug-resistant microbes, it is highly urgent to build more efficient antimicrobial methods with minor drug-resistance. Recently, with the efforts of scientists, various antibacterial strategies have been designed and constructed for bacterial infections treatment, such as photodynamic therapy (PDT),[9–11] photothermal therapy (PTT)[12–19] and chemodynamic therapy (CDT),[20,21] *etc.* As an emerging and potential strategy, CDT can trigger the Fenton reaction which converts $H_2O_2$ to generate •OH with much stronger oxidizability. •OH can effectively destroy the lipoproteins of the bacterial cell wall, which would lead to the death of pathogens and achieve antimicrobial activity. In the past decades, quite a lot of nanomaterials have been employed as Fenton or Fenton-like catalysts to enrich the establishment of CDT-based nanosystems, such as transition metal ions, metal-based nanomaterials or graphene oxide.[22–27] Nonetheless, the efficiency of CDT is also restricted by some other factors. Generally, endogenous $H_2O_2$ concentrations and pH microenvironment ranges usually can't meet the demand of the Fenton reaction, which greatly limits the further efficiency and further applications of CDT. With the rapid development of nanoscience and nanotechnology, scientists have put forward the strategy of cooperating glucose oxidase (GOx) and Fenton catalysts to resolve the problem. As is known to all, GOx is capable of catalyzing glucose into gluconic acid and $H_2O_2$, which are the essential elements for the subsequent Fenton reaction. However, due to the intrinsic properties of enzymes, establishing nanosystems to immobilize GOx and maintain the enzyme catalytic activity at a maximum at the same time has been the top priority.

Polymer capsules with stable structures have attracted much interest from researchers and have been utilized to play a role in a broad range of application fields, such as cargo loading, bioimaging and nanoreactors for catalysis.[28–33] Covalent assembly is a facile and template-free strategy to construct polymer capsules based on building blocks with multiple reactive groups. In this way, various functionalized macrocyclic host molecules, such as cucurbiturils, cyclodextrins and pillarenes, can be utilized for covalent assembly to construct polymer capsules, which greatly enrich the selectivity of the building blocks. Besides, further modification at the surface of polymer capsules can be realized to build more sophisticated structures, which would greatly extend the function and application fields. Therefore, polymer capsules can be an appropriate alternative to efficiently

[a] State Key Laboratory of Supramolecular Structure and Materials, College of Chemistry, Jilin University, Changchun 130012, People's Republic of China. E-mail: junqiuliu@jlu.edu.cn, xujiayun@jlu.edu.cn
[b] College of Material, Chemistry and Chemical Engineering, Hangzhou Normal University, and Key Laboratory of Organosilicon Chemistry and Material Technology, Ministry of Education, Hangzhou, China

† Electronic supplementary information (ESI) available. See DOI: 10.1039/d1tb00868d

‡ These authors contributed equally to this work.

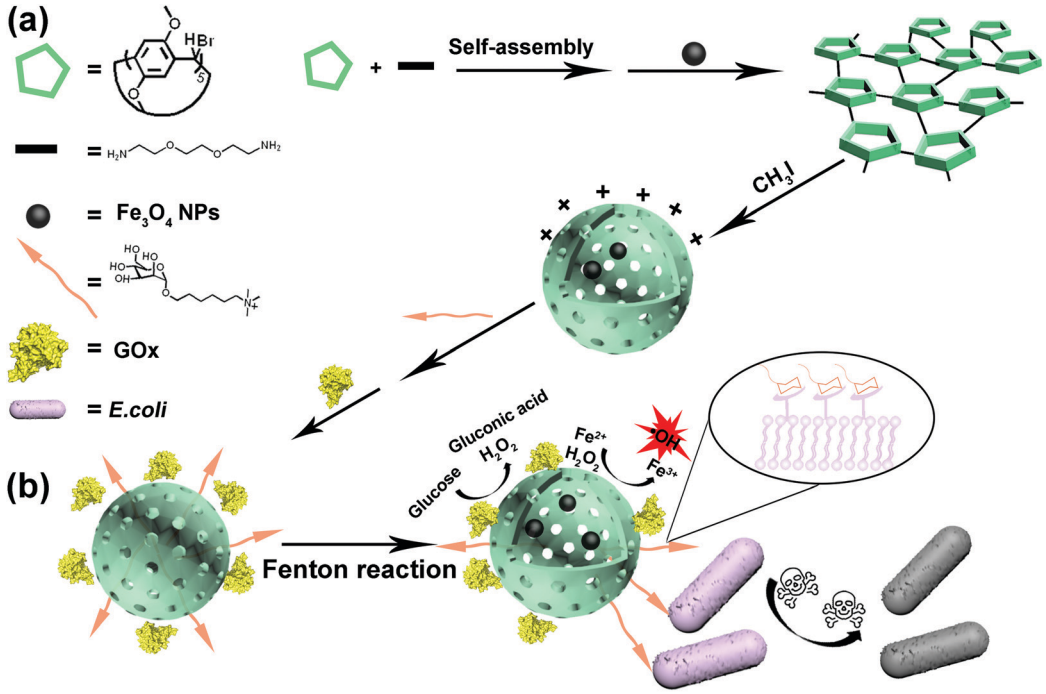


Scheme 1 (a) Schematic diagram of the preparation of the covalent-assembled polymer capsules. (b) The antibacterial CDT process of the cascade catalytic nanoplatform.

encapsulate Fenton catalysts and immobilize GOx for the establishment of a cascade catalytic nanoplatform.

Herein, a cascade catalytic nanoplatform (GOx–NCs/$Fe_3O_4$) was constructed by the covalent assembly of laterally-modified pillar[5]arenes (BDMP5) for antibacterial CDT toward *Escherichia coli* (*E. coli*). Polymer capsules encapsulating $Fe_3O_4$ nanoparticles (NCs/$Fe_3O_4$) were prepared through covalent co-assembly of BDMP5 and a flexible linker (Scheme 1). The polymer capsules could be positively charged by further methylation with secondary amines. The positively charged capsule could absorb negatively charged GOx onto its surface to form the nanocomplex GOx–NCs/$Fe_3O_4$. In the presence of glucose, GOx could firstly catalyze it into gluconic acid and $H_2O_2$, which would trigger $Fe_3O_4$ nanoparticles to release $Fe^{2+}$. Subsequently, $Fe^{2+}$ would further catalyze $H_2O_2$ into highly toxic •OH *via* the Fenton reaction, destroying bacterial outer membrane structures and causing the death of bacteria. More importantly, quaternary ammonium decorated with mannose could be non-covalently modified at the surface of the polymer capsules through host–guest interactions with BDMP5. By this means, water-solubility and biocompatibility of the nanoplatform would be greatly improved. Furthermore, the binding interactions between mannose and *E. coli* were also beneficial for realizing an enhanced antibacterial CDT effect.

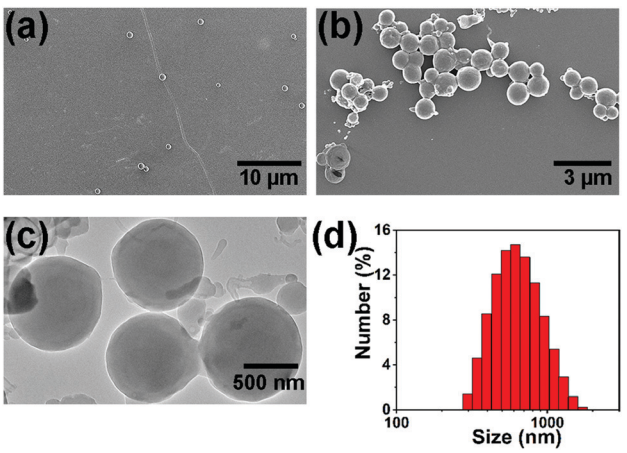


Fig. 1 (a and b) SEM images, (c) TEM image and (d) DLS results of the polymer capsules.

## Results and discussion

The resulting capsules were firstly characterized by scanning electron microscopy (SEM), transmission electron microscopy (TEM) and dynamic light scattering (DLS) to observe the morphologies. As shown in Fig. 1, the polymer capsules were well regulated and had hollow interior structures with an average diameter of 800 nm, the size of which was appropriate for nanoparticles encapsulation and for acting as nanoreactors for cascade catalysis. Moreover, as shown in Fig. S11 (ESI†), the Fourier transform infrared spectroscopy (FTIR) spectrum revealed that the absorption band at 676 $cm^{-1}$ consistent with C–Br stretching disappeared and the absorption band at 3300 $cm^{-1}$ consistent with C–N stretching appeared, demonstrating the covalent cross-linking of BDMP5. All the results indicated that polymer capsules were successfully prepared by covalent assembly of BDMP5.

 

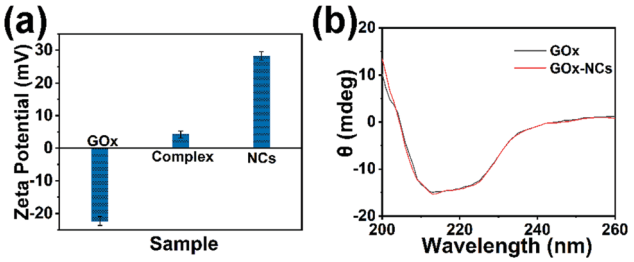


Fig. 2 (a) Zeta potential and (b) CD spectra of GOx, NCs and GOx–NCs complex.

GOx was absorbed onto the surface of the methylated polymer capsules to form a nanocomplex through electrostatic interactions. This process was monitored using zeta potential measurements. As shown in Fig. 2a, the methylated polymer capsules exhibited a positively charged surface, of which the zeta potential value decreased when mixed with negatively charged GOx. The process of the Fenton reaction required maintaining of the protein activity and catalytic activity. Circular dichroism (CD) spectroscopy was utilized to investigate the secondary structure of GOx and GOx–NCs. As shown in Fig. 2b, the conformation of GOx didn't changed after the formation of the nanocomplex, indicating that electrostatic adsorption wouldn't leading to the protein denaturation.

Efficient Fenton reaction required the GOx–NCs to maintain high catalytic ability. The catalytic ability of GOx–NCs was evaluated by the generation of $H_2O_2$ and gluconic acid. As shown in Fig. 3a, the pH value decreased with the increase in glucose concentrations incubated with GOx–NCs. When the glucose concentration was at 5 mmol, the pH value could decrease below 4, and this range was appropriate for the Fenton reaction.

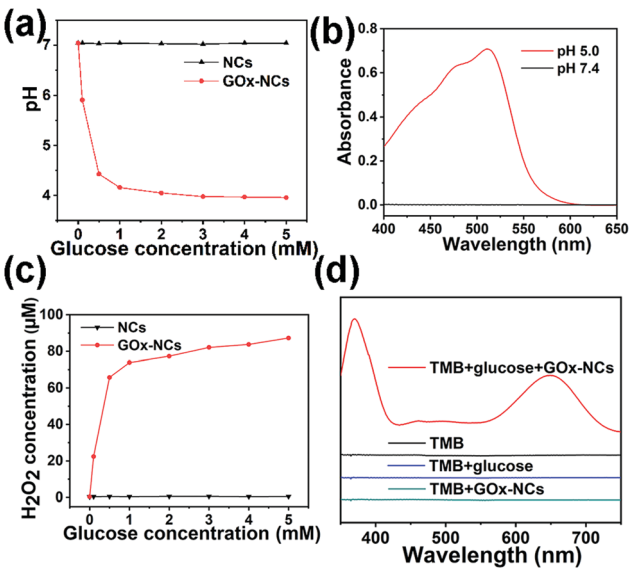


Fig. 3 (a) pH values and (c) $H_2O_2$ concentration of GOx–NCs and NCs under different glucose concentrations. (b) UV-vis spectra of *o*-phenanthroline incubated with NCs/$Fe_3O_4$ under different pH conditions. (d) UV-vis spectra of TMB solution incubated with different samples.

Besides, $Fe^{2+}$ was detected by measuring the ultraviolet-visible (UV-vis) absorbance peak of *o*-phenanthroline incubated with NCs/$Fe_3O_4$ in different pH environments (Fig. 3b), which would form a complex with $Fe^{2+}$. The $H_2O_2$ concentration also increased with the increase in glucose concentrations incubated with GOx–NCs (Fig. 3c), overcoming the problem of insufficient endogenous $H_2O_2$ amount. And $H_2O_2$ was detected by measuring the UV-vis absorbance peak of tetramethylbenzidine (TMB) solution incubated with GOx–NCs and glucose (Fig. 3d). All the above results demonstrated that GOx–NCs had an excellent catalytic ability towards glucose.

Generated $^{\bullet}OH$ was detected by UV-vis spectroscopy and electron spin resonance (ESR) spectroscopy. Methylene blue (MB) could be degraded by the generated $^{\bullet}OH$, resulting in the decrease of the absorption peak at 664 nm. When MB solution was mixed with the GOx–NCs/$Fe_3O_4$ nanoplatform, the absorption band of MB greatly decreased once glucose was added and incubated with the solution (Fig. 4a). In addition, the characteristic signal of $^{\bullet}OH$ could be directly observed by ESR spectroscopy when GOx–NCs/$Fe_3O_4$ was incubated with glucose (Fig. 4b). All the results indicated the occurrence of the Fenton reaction during the cascade catalytic process.

The antimicrobial CDT performance of the nanoplatform was evaluated by plate counting. *E. coli* was incubated with different samples at different conditions and seeded onto LB solid agar medium by plate coating. As shown in Fig. 5, glucose wouldn't inhibit the growth of bacteria. GOx, GOx–NCs and GOx–NCs/$Fe_3O_4$ wouldn't result in the inhibition of bacteria when incubated without glucose. GOx, GOx–NCs and GOx–NCs/$Fe_3O_4$ exhibited obvious inhibition towards *E. coli* when incubated with glucose. And the inhibition ratio was related with the concentration of GOx and $Fe_3O_4$ nanoparticles. When incubated with glucose and at the same concentrations, GOx–NCs/$Fe_3O_4$ exhibited much higher inhibition efficiency towards *E. coli* than GOx and GOx–NCs. The real-time $OD_{600}$ values of the bacterial suspensions after treatment were recorded to explore the antibacterial activity of the samples in solution. The $OD_{600}$ values of the bacterial suspensions after the treatment with GOx–NCs/$Fe_3O_4$ didn't increase over time. All these results demonstrated that $^{\bullet}OH$ generated by the GOx–NCs/$Fe_3O_4$ nanoplatform showed highly efficient antibacterial efficiency towards *E. coli*.

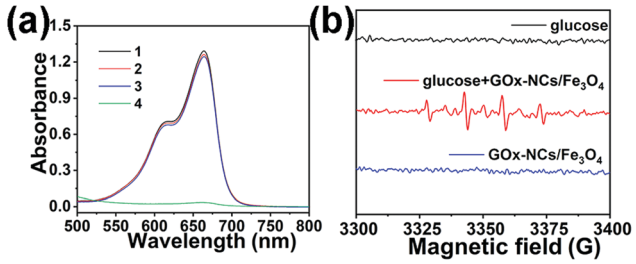


Fig. 4 (a) UV-vis spectra of MB solutions after incubations with different samples. (1): MB solution; (2): MB incubated with GOx–NCs/$Fe_3O_4$; (3): MB incubated with GOx–NCs and glucose; (4): MB incubated with GOx–NCs/$Fe_3O_4$ and glucose. (b) ESR signals of different samples after incubation.

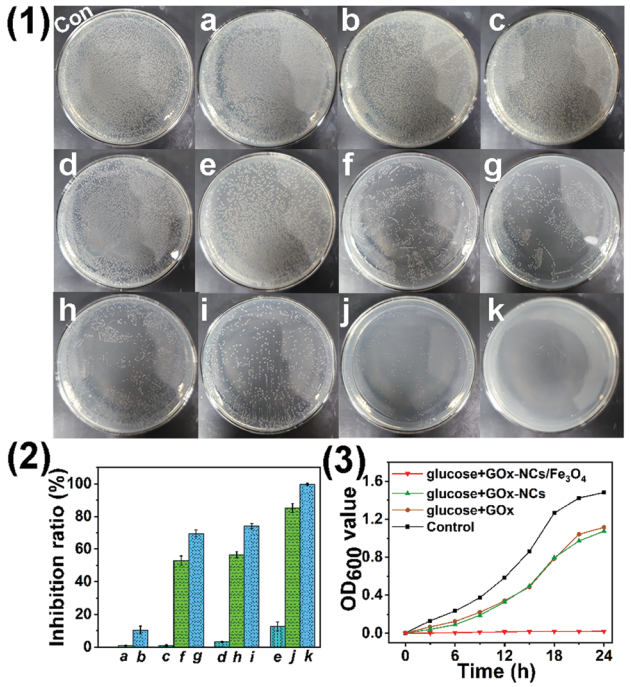


Fig. 5 (1) Plate coating results, (2) bacterial inhibition rates and (3) real-time $OD_{600}$ values of different treatments towards *E. coli*. The glucose concentration was 5 mmol. (a): glucose. (b): NCs. (c): GOx (10 μg $mL^{-1}$) without glucose. (d and e): GOx–NCs (10 μg $mL^{-1}$) and GOx–NCs/$Fe_3O_4$ (GOx: 10 μg $mL^{-1}$; $Fe_3O_4$: 50 μg $mL^{-1}$) without glucose. (f and g): GOx (5 μg $mL^{-1}$ and 10 μg $mL^{-1}$) incubated with glucose. (h and i): GOx–NCs (5 μg $mL^{-1}$ and 10 μg $mL^{-1}$) incubated with glucose. (j) GOx–NCs/$Fe_3O_4$ (GOx: 5 μg $mL^{-1}$ and $Fe_3O_4$: 25 μg $mL^{-1}$) and (k): GOx–NCs/$Fe_3O_4$ (GOx: 10 μg $mL^{-1}$ and $Fe_3O_4$ 50 μg $mL^{-1}$) incubated with glucose.

SEM and confocal laser scanning microscopy (CLSM) measurements were conducted to investigate the antibacterial mechanism of the nanoplatform based on CDT. SEM was utilized to observe the morphologies of *E. coli* incubated with different samples. As shown in Fig. 6, glucose didn't influence the morphologies of *E. coli*. Meanwhile, the morphologies of *E. coli* incubated with GOx–NCs/$Fe_3O_4$ didn't change, either. In contrast, once the glucose was added and incubated with GOx–NCs/$Fe_3O_4$, obvious serious damage to the *E. coli* morphologies was observed.

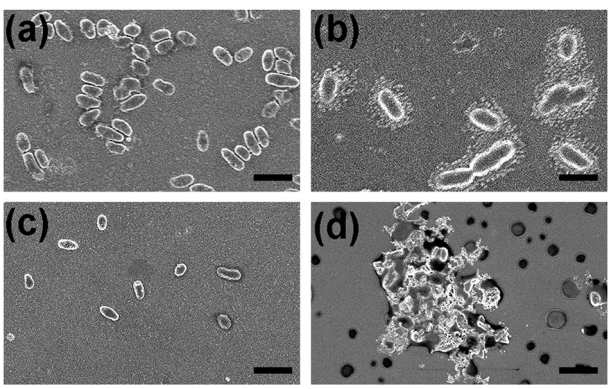


Fig. 6 The morphologies of *E. coli* after different treatments: (a) control; (b) glucose; GOx–NCs/$Fe_3O_4$ incubated (c) without glucose and (d) with glucose. Scale bar: 1 μm.

Bacterial suspensions were incubated with PI solution after treatment. PI could embed into the ruptured bacterial membrane and bind with DNA to exhibit red fluorescence. CLSM were used to observe the fluorescence signal of PI. As shown in Fig. 7, a strong fluorescence signal was observed after the treatment with GOx–NCs/$Fe_3O_4$ and glucose. This indicated that the bacterial membrane of *E. coli* was badly destroyed by generated $^{\bullet}OH$. With the breaking of the membrane, *E. coli* was efficiently inhibited by CDT.

In the end, the cytotoxity of the polymer capsules was explored using the methyl thiazolyl tetrazolium (MTT) assay. NIH/3T3 cells were chosen as the model, and the cytotoxity of the polymer capsules was tested at different concentrations. As shown in Fig. 8, the polymer capsules showed little to no cytotoxity even at higher concentrations. This result demonstrated that the polymer capsules had good biocompatibility, which held great promise for use as nanocarriers for biomedical applications.

## Experimental

### Synthesis of the Man-DMA

1,2,3,4,6-Penta-*O*-acetyl-α-D-mannopyranoside (540 mg, 1.4 mmol) was dissolved in $CH_2Cl_2$(7 mL), then 6-bromo-1-hexanol (370 μL) and $BF_3{\cdot}Et_2O$ (870 μL) were added into the solution. The mixture was kept stirring at room temperature for 20 h. After being diluted with $CH_2Cl_2$, the mixture was then washed with deionized water, a saturated solution of $NaHCO_3$ and finally deionized water again. Being collected and dried over $Na_2SO_4$, the organic layer was concentrated to obtain the crude product, which was purified by column chromatography to obtain compound **1**. Subsequently compound **1** (256 mg, 0.5 mmol), dissolved in acetonitrile (15 mL), was mixed with trimethylamine (1 mL). After being heated to reflux overnight, the mixture was concentrated to obtain the crude product, which was washed with $CH_2Cl_2$ and dried to obtain compound **2**. Subsequently compound **2** (114 mg, 0.2 mmol) was dissolved in methanol and mixed with sodium methanolate (5.4 mol $L^{-1}$, 50 μL). The mixture was stirred overnight and neutralized with Amberlite. The neutralized solution was carefully filtered and concentrated to obtain the final product Man-DMA.

### Synthesis of pillar[5]arene-based polymer capsules (NCs) and polymer capsules encapsulating $Fe_3O_4$ nanoparticles (NCs/$Fe_3O_4$)

The synthesis of BDMP5 was based on previously published work by our team.[34] BDMP5 (30 mg) and 1,2-bis(2-aminoethoxy)ethane (20.0 μL) were dissolved in methanol (30.0 mL). Then the solution was stirred at 50 °C for 5 h under nitrogen atmosphere. Subsequently the mixture was dialyzed against DMF for 24 h to remove the unreacted reactants. Next adding iodomethane (500 μL) and excessive potassium carbonate into the solution, the mixture was stirred at room temperature overnight. Then the

 

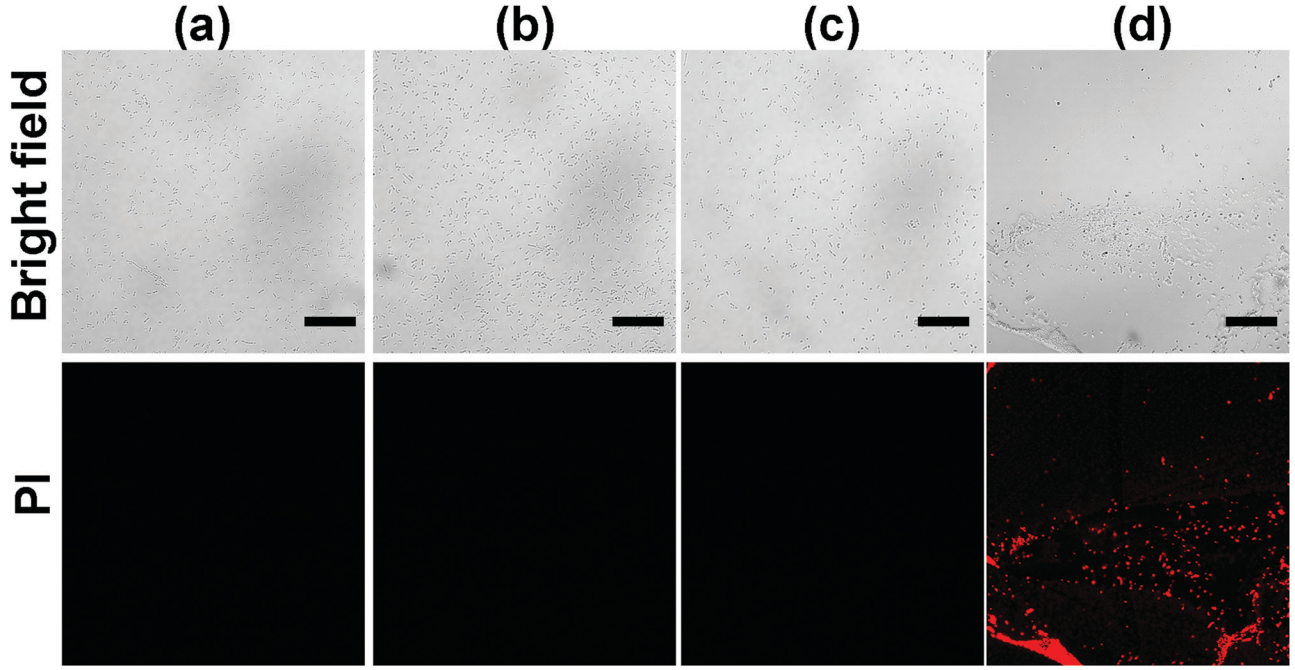


Fig. 7 Confocal laser scanning microscopy images of *E. coli* after different treatments: (a) control; (b) glucose; GOx–NCs/$Fe_3O_4$ incubated (c) without glucose and (d) with glucose. Scale bar: 20 μm.

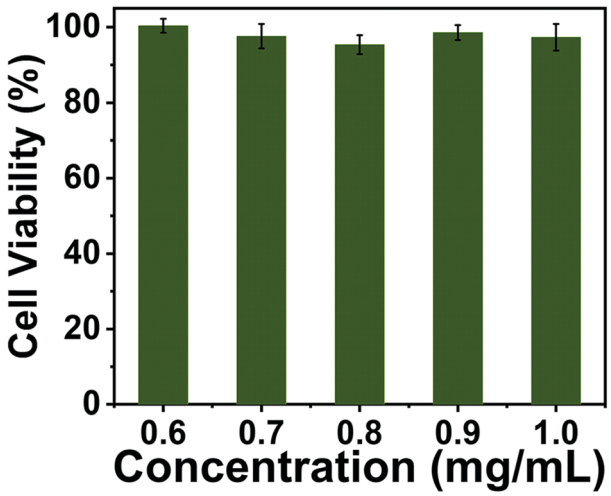


Fig. 8 Cell viability of NIH/3T3 cells incubated with polymer capsules at different concentrations.

solution was dialyzed against DMF and deionized water for 24 h to remove the unreacted reactants and solvents to obtain the polymer capsules. Man-DMA, dissolved in water, was added into the solution which was sonicated for two hours to achieve the host–guest complexation. NCs/$Fe_3O_4$ was synthesized with the presence of dispersed $Fe_3O_4$ nanoparticles.

### Preparation of nanocomplex (GOx–NCs) and zeta potential experiments

GOx–NCs was prepared by the mixing and co-incubating of NCs and GOx, the nanocomplex was diluted to obtain different concentrations (5 μg $mL^{-1}$ and 10 μg $mL^{-1}$). The zeta potentials of GOx, NCs and GOx–NCs were tested by DLS.

### Catalytic ability of GOx–NCs

The CD experiments were carried out firstly to explore the structure changes of GOx and GOx–NCs. The catalytic ability was measured at different glucose concentrations when incubated with GOx–NCs. After incubation, the pH values were measured using a pH meter and the $H_2O_2$ concentration was determined using a Micro Hydrogen Peroxide ($H_2O_2$) Assay Kit.

### Detection of $H_2O_2$

The detection of $H_2O_2$ was determined by measuring the UV-vis absorbance peak of tetramethylbenzidine solution incubated with GOx–NCs and glucose.

### The release of $Fe^{2+}$

The release of $Fe^{2+}$ was evaluated by measuring the UV-vis absorbance peak of *o*-phenanthroline incubated with NCs/$Fe_3O_4$ in different pH environments (pH 5.0 and 7.4).

### Synthesis of catalytic nanoplatform (GOx–NCs/$Fe_3O_4$) and $^{\bullet}OH$ generation ability

GOx was dissolved in water and mixed with NCs/$Fe_3O_4$ to build the catalytic nanoplatform. The catalytic nanoplatform was diluted to obtain different concentrations. GOx–NCs/$Fe_3O_4$ was incubated with methylene blue in the presence of glucose. The generation of $^{\bullet}OH$ was determined by the absorbance of methylene blue at 664 nm. Moreover, the generation of $^{\bullet}OH$ was also proved by ESR spectroscopy with DMPO as a trapping agent.

### Bacterial culture and antibacterial experiments

*E. coli* was diluted into 6 mL LB culture medium and cultured at 37 °C overnight. When the $OD_{600}$ value reached 0.8, the bacteria were collected, washed, diluted and resuspended in 0.9% sodium chloride solution. The bacterial suspension was mixed and incubated with GOx–NCs/$Fe_3O_4$ and GOx–NCs at different concentrations in the presence of glucose for 4 h. Next 100 μL suspension solution was dispersed on solid LB plates and cultured at 37 °C overnight. The bacterial inhibition ratio was then calculated based on the counting of bacterial colonies.

### Bacterial morphology

SEM was used to observe the morphology of *E. coli* after antibacterial experiments. Bacterial suspensions were dropped onto hydroxylated silicon wafers and dried at room temperature. Then the dried samples were fixed by glutaraldehyde for thirty minutes and washed twice with ultrapure water. Finally, ethanol of different mass fractions was dropped onto the hydroxylated silicon wafers to dehydrate the bacteria samples.

### CLSM experiments

*E. coli* after antibacterial experiments was tested using CLSM. 200 μL Bacterial suspensions were incubated with 20 μL PI solution (10 μg $mL^{-1}$) in a constant-temperature incubator for forty minutes. The bacterial suspensions were then centrifuged and resuspended. The resuspended bacterial suspensions were dropped on glass slides and covered by cover slips.

### Cytotoxicity tests

The cytotoxicity of the polymer capsules was evaluated using the MTT assay. NIH/3T3 cells were cultured with RPMI 1640 culture medium containing 10% fetal bovine serum. A 96-well plate was seeded with 3T3 cells at a density of 7000. Polymer capsules of different concentrations were incubated with the cells for 24 h. 15 μL MTT solution was added into the 96-well plate and incubation was continued for 4 h. Subsequently the culture medium was removed and DMSO added. The absorbance of the dissolved solution was determined on a microplate reader.

## Conclusions

A highly efficient cascade catalytic nanoplatform was successfully established by a facile strategy. Positively charged polymer capsules were prepared by the covalent self-assembly of BDMP5 and methylation modification, which could encapsulate $Fe_3O_4$ nanoparticles effectively and absorb GOx on the surface to build the nanoplatform. Maintaining the enzymatic activity of GOx, the platform could catalyze glucose efficiently and trigger cascade catalytic Fenton reaction to generate highly oxidative $^{\bullet}OH$. The generated $^{\bullet}OH$ caused severe damage to bacterial structures and morphology so as to realize chemodynamic antibacterial therapy towards *E. coli* at a low concentration. Furthermore, the polymer capsules displayed excellent biocompatibility to mammalian cells, which would hold huge potential for the construction of more and safe nanosystems to apply in biomedical fields.

## Conflicts of interest

There are no conflicts to declare.

## Acknowledgements

This work was supported by the National Key R&D Program of China (Grant No. 2018YFA0901600, No. 2020YFA0908500), and National Natural Science Foundation of China (No. 22001054, 22075065).

## Notes and references

1 W. Kim, W. Zhu, G. L. Hendricks, D. Van Tyne, A. D. Steele, C. E. Keohane, N. Fricke, A. L. Conery, S. Shen, W. Pan, K. Lee, R. Rajamuthiah, B. B. Fuchs, P. M. Vlahovska, W. M. Wuest, M. S. Gilmore, H. Gao, F. M. Ausubel and E. Mylonakis, *Nature*, 2018, **556**, 103–107.
2 L. Zhou, H. Zheng, Z. Liu, S. Wang, Z. Liu, F. Chen, H. Zhang, J. Kong, F. Zhou and Q. Zhang, *ACS Nano*, 2021, **15**, 2468–2480.
3 T. Lawes, J.-M. Lopez-Lozano, C. A. Nebot, G. Macartney, R. Subbarao-Sharma, C. R. J. Dare, K. D. Wares and I. M. Gould, *Lancet Infect. Dis.*, 2015, **15**, 1438–1449.
4 A. Y. Peleg and D. C. Hooper, *N. Engl. J. Med.*, 2010, **362**, 1804–1813.
5 B. Allegranzi, S. B. Nejad, C. Combescure, W. Graafmans, H. Attar, L. Donaldson and D. Pittet, *Lancet*, 2011, **377**, 228–241.
6 V. D. Rosenthal, *Lancet*, 2011, **377**, 186–188.
7 K. Rutledge-Taylor, A. Matlow, D. Gravel, J. Embree, N. Le Saux, L. Johnston, K. Suh, J. Embil, E. Henderson, M. John, V. Roth, A. Wong, J. Shurgold and G. Taylor, *Am. J. Infect. Control*, 2012, **40**, 491–496.
8 M. F. Richter, B. S. Drown, A. P. Riley, A. Garcia, T. Shirai, R. L. Svec and P. J. Hergenrother, *Nature*, 2017, **545**, 299–304.
9 D. Wang, L. Niu, Z.-Y. Qiao, D.-B. Cheng, J. Wang, Y. Zhong, F. Bai, H. Wang and H. Fan, *ACS Nano*, 2018, **12**, 3796–3803.
10 Y. Li, Z. Zhao, J. Zhang, R. T. K. Kwok, S. Xie, R. Tang, Y. Jia, J. Yang, L. Wang, J. W. Y. Lam, W. Zheng, X. Jiang and B. Z. Tang, *Adv. Funct. Mater.*, 2018, **28**, 1804632.
11 K. Liu, Y. Liu, Y. Yao, H. Yuan, S. Wang, Z. Wang and X. Zhang, *Angew. Chem., Int. Ed.*, 2013, **52**, 8285–8289.
12 G. Qing, X. Zhao, N. Gong, J. Chen, X. Li, Y. Gan, Y. Wang, Z. Zhang, Y. Zhang, W. Guo, Y. Luo and X.-J. Liang, *Nat. Commun.*, 2019, **10**, 4336.
13 Y. Wang, S. Li, L. Liu and L. Feng, *ACS Appl. Bio Mater.*, 2018, **1**, 27–32.
14 Y. Feng, Q. Chen, Q. Yin, G. Pan, Z. Tu and L. Liu, *ACS Appl. Bio Mater.*, 2019, **2**, 747–756.
15 C. J. Jeong, S. M. Sharker, I. In and S. Y. Park, *ACS Appl. Mater. Interfaces*, 2015, **7**, 9469–9478.
16 S. H. Kim, E. B. Kang, C. J. Jeong, S. M. Sharker, I. In and S. Y. Park, *ACS Appl. Mater. Interfaces*, 2015, **7**, 15600–15606.

 

17 W. Yin, J. Yu, F. Lv, L. Yan, L. R. Zheng, Z. Gu and Y. Zhao, *ACS Nano*, 2016, **10**, 11000–11011.
18 Y.-Q. Zhao, Y. Sun, Y. Zhang, X. Ding, N. Zhao, B. Yu, H. Zhao, S. Duan and F.-J. Xu, *ACS Nano*, 2020, **14**, 2265–2275.
19 J. T. Robinson, S. M. Tabakman, Y. Liang, H. Wang, H. Sanchez Casalongue, D. Vinh and H. Dai, *J. Am. Chem. Soc.*, 2011, **133**, 6825–6831.
20 F. Gao, X. Li, T. Zhang, A. Ghosal, G. Zhang, H. M. Fan and L. Zhao, *J. Controlled Release*, 2020, **324**, 598–609.
21 B. C. Kim, E. Jeong, E. Kim and S. W. Hong, *Appl. Catal., B*, 2019, **242**, 194–201.
22 Y. Liu, W. Zhen, L. Jin, S. Zhang, G. Sun, T. Zhang, X. Xu, S. Song, Y. Wang, J. Liu and H. Zhang, *ACS Nano*, 2018, **12**, 4886–4893.
23 P. a. Ma, H. Xiao, C. Yu, J. Liu, Z. Cheng, H. Song, X. Zhang, C. Li, J. Wang, Z. Gu and J. Lin, *Nano Lett.*, 2017, **17**, 928–937.
24 J. Kim, H. R. Cho, H. Jeon, D. Kim, C. Song, N. Lee, S. H. Choi and T. Hyeon, *J. Am. Chem. Soc.*, 2017, **139**, 10992–10995.
25 F. Cao, Y. Zhang, Y. Sun, Z. Wang, L. Zhang, Y. Huang, C. Liu, Z. Liu, J. Ren and X. Qu, *Chem. Mater.*, 2018, **30**, 7831–7839.
26 S.-Y. Yin, G. Song, Y. Yang, Y. Zhao, P. Wang, L.-M. Zhu, X. Yin and X.-B. Zhang, *Adv. Funct. Mater.*, 2019, **29**, 1901417.
27 C. Liu, J. Xing, O. U. Akakuru, L. Luo, S. Sun, R. Zou, Z. Yu, Q. Fang and A. Wu, *Nano Lett.*, 2019, **19**, 5674–5682.
28 C. Sun, H. Zhang, L. Yue, S. Li, Q. Cheng and R. Wang, *ACS Appl. Mater. Interfaces*, 2019, **11**, 22925–22931.
29 C. Sun, L. Yue, Q. Cheng, Z. Wang and R. Wang, *ACS Mater. Lett.*, 2020, **2**, 266–271.
30 Y. Li, M. Wu, B. Wang, Y. Wu, M. Ma and X. Zhang, *ACS Sustainable Chem. Eng.*, 2016, **4**, 5523–5532.
31 D. Kim, E. Kim, J. Lee, S. Hong, W. Sung, N. Lim, C. G. Park and K. Kim, *J. Am. Chem. Soc.*, 2010, **132**, 9908–9919.
32 R. Liu, J. Zhao, Q. Han, X. Hu, D. Wang, X. Zhang and P. Yang, *Adv. Mater.*, 2018, **30**, 1802851.
33 K. C. Bentz and D. A. Savin, *Polym. Chem.*, 2018, **9**, 2059–2081.
34 S. Fu, G. An, H. Sun, Q. Luo, C. Hou, J. Xu, Z. Dong and J. Liu, *Chem. Commun.*, 2017, **53**, 9024–9027.